

Self-learning Local Supervision Encoding Framework to Constrict and Disperse Feature Distribution for Clustering

Jielei Chu, Tianrui Li, *Senior member, IEEE*, Hongjun Wang, Jing Liu and Meng Hua

arXiv:1812.01967v1 [cs.LG] 5 Dec 2018

Abstract—To obtain suitable feature distribution is a difficult task in machine learning, especially for unsupervised learning. In this paper, we propose a novel self-learning local supervision encoding framework based on RBMs, in which the self-learning local supervisions from visible layer are integrated into the contrastive divergence (CD) learning of RBMs to constrict and disperse the distribution of the hidden layer features for clustering tasks. In the framework, we use sigmoid transformation to obtain hidden layer and reconstructed hidden layer features from visible layer and reconstructed visible layer units during sampling procedure. The self-learning local supervisions contain local credible clusters which stem from different unsupervised learning and unanimous voting strategy. They are fused into hidden layer features and reconstructed hidden layer features. For the same local clusters, the hidden features and reconstructed hidden layer features of the framework tend to constrict together. Furthermore, the hidden layer features of different local clusters tend to disperse in the encoding process. Under such framework, we present two instantiation models with the reconstruction of two different visible layers. One is self-learning local supervision GRBM (slsGRBM) model with Gaussian linear visible units and binary hidden units using linear transformation for visible layer reconstruction. The other is self-learning local supervision RBM (slsRBM) model with binary visible and hidden units using sigmoid transformation for visible layer reconstruction. The experimental results prove that the hidden layer features of slsGRBM and slsRBM show better clustering performance due to more reasonable distribution than original data in the Microsoft Research Asia Multimedia (MSRA-MM)2.0 dataset and UCI datasets, respectively. Furthermore, the experiments demonstrate that the self-learning local supervisions bring more positive impact for feature extraction of slsGRBM and slsRBM model than traditional GRBM and RBM without any external interventions, respectively.

Keywords—restricted Boltzmann machine; feature extraction; CD learning; unsupervised clustering.

I. INTRODUCTION

Feature extraction is currently the subject of intense research because of its wide applications. In many applications, like visual recognition[1], scene analysis[2], [3], object recognition[4], multimodal learning[5], [6], speech recognition[7], image classification[8] and activity recognition[9], feature learning is not only an essential phase but a crucial procedure which is used to simplify the subsequent tasks by obtaining appropriate features distribution from

the input data.

Many modeling paradigms such as autoencoders and energy-based models have been applied to feature learning. The restricted Boltzmann machine (RBM)[10] is a popular energy-based model for unsupervised feature learning and aims to explore appropriate hidden features. The structure of an RBM is a bipartite graph consists of a binary visible layer and a binary hidden layer. There are no connections between the interior of visible layer units and the interior of hidden layer units. The most popular learning algorithms of RBM such as stochastic maximum likelihood[11] and contrastive divergence (CD)[12] base on the efficient Gibbs sampling. There are a large number of successful applications based on the RBMs, e.g., speaker recognition[7], feature fusion[6], clustering[13], natural language understanding[14], classification[15], [16], [17], [18], [19], computer vision[20] and speech recognition[21]. Meanwhile, various variants of the RBMs have been proposed by the researchers, e.g., pairwise constraints restricted Boltzmann machine with Gaussian visible units (pcGRBM)[22], classification RBM[23], fuzzy restricted Boltzmann machine (FRBM)[24], sparse restricted Boltzmann machine (SRBM)[25] and spike-and-slab restricted Boltzmann machine (ssRBM)[26]. For real-valued data, the RBM with Gaussian visible units[5], [22] as the canonical energy model has usually been applied to extract the hidden features from image data. Unlike standard RBM, the visible layer units of the model have Gaussian noise and the hidden layer still maintains binary units. The CD learning can also be used to train the RBM with Gaussian visible units[27]. The hidden representations of traditional RBMs do not have explicit instance-level constraints. So, Chu et al. presented semi-supervised pcGRBM that pairwise constraints are fused into the reconstructed visible layer[22]. However, the labeled data is lacking in many applications and it is expensive to obtain more labels. So, it is certainly worth exploring unsupervised feature learning method of RBMs by fusing external interventions.

To obtain suitable feature distribution is a difficult task in machine learning, especially for unsupervised learning. In our previous research[22], we have explored semi-supervised feature extraction based on GRBM. In this paper, we explore further unsupervised feature extraction based on RBMs to constrict and disperse hidden layer feature distribution for clustering tasks. Some self-learning local supervisions from visible layer are integrated into the contrastive divergence (CD) learning in the hidden layer and reconstructed hidden

Jielei Chu, Tianrui Li, Hongjun Wang, Hua Meng are with the School of Information Science and Technology, Southwest Jiaotong University, Chengdu, 611756, Sichuan, China. e-mails: {jieleichu, trli, wanghongjun, huameng}@swjtu.edu.cn.

Jing Liu is with the School of Business, Sichuan University, Sichuan, 610065, Chengdu, China. e-mail: liujing@scu.edu.cn

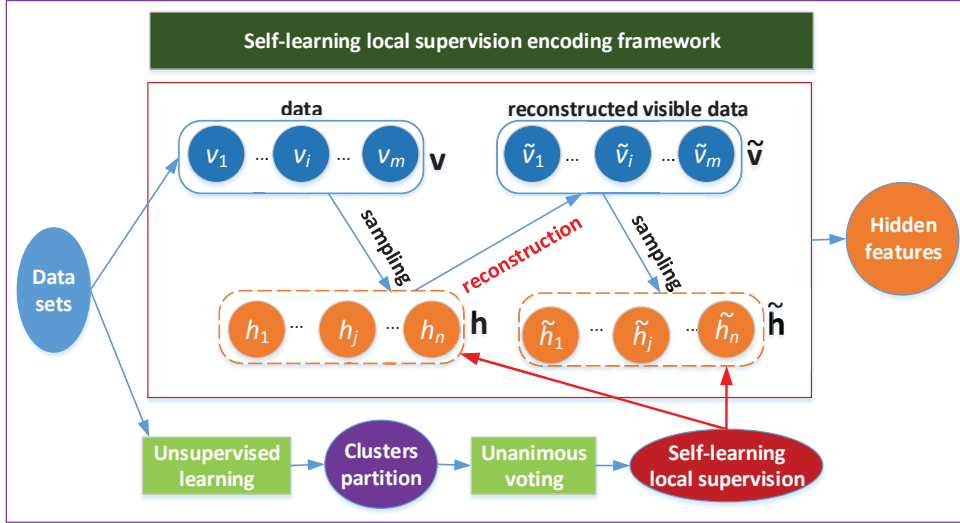


Fig. 1. The self-learning local supervisions from visible layer are integrated into hidden layer and reconstructed hidden layer of the contrastive divergence (CD) learning of RBMs. In the encoding procedure, we use sigmoid transformation to obtain the hidden layer features and the reconstructed hidden layer features during sampling procedure. In the reconstruction procedure, we use linear transformation to obtain the reconstructed visible layer units from the hidden layer units that is an instantiation model of self-learning local supervision GRBM (slsGRBM) with Gaussian linear visible units and binary hidden units. Similarly, we use sigmoid transformation to obtain the reconstructed visible layer units from the hidden layer units that is an instantiation model of self-learning local supervision RBM (slsRBM) with binary visible units and hidden units.

layer, then we propose a novel encoding framework. The self-learning local supervisions stem from unsupervised learning and unanimous voting strategy. They are fused into hidden layer features and reconstructed hidden layer features. Under such a framework, we propose two instantiation models: one is self-learning local supervision GRBM (slsGRBM) with Gaussian linear visible units and binary hidden units for modeling real-valued data and the other is self-learning local supervision RBM (slsRBM) with binary visible units and hidden units using different transformations for visible layer reconstruction. The contributions of our work are summarized below.

- A novel self-learning local supervision encoding framework is presented in which the self-learning local supervisions from visible layer are integrated into the CD learning of RBMs to constrict and disperse the distribution of the hidden layer features and reconstructed hidden layer features.
- An instantiation model of self-learning local supervision GRBM (slsGRBM) with Gaussian linear visible units and binary hidden units is proposed using linear transformation for visible layer reconstruction under our encoding framework.
- An instantiation model of self-learning local supervision RBM (slsRBM) with binary visible units and hidden units based on our encoding framework is proposed using sigmoid transformation for visible layer reconstruction.
- We demonstrate that the self-learning local supervisions bring more positive impact for feature extraction of slsGRBM and slsRBM model than traditional GRBM on the MSRA-MM 2.0 image data and RBM on UCI data sets without any external interventions using unsupervised clustering, respectively.

The remaining of the paper is organized as follows. The related work is provided in Section II. In Section III, the theoretical background is described. The self-learning local supervisions encoding framework and the learning algorithm of two instantiation models slsGRBM and slsRBM are proposed in Section IV. The experimental results are shown in Section V. Finally, our contributions are summarized in Section VI.

II. RELATED WORK

In this section, we review literature on supervised, semi-supervised, unsupervised feature learning based on RBMs and other models, together with the voting strategy in supervised learning.

Supervised feature learning has proved to be an effective method in machine learning[8], [28], [29], [15], [30], [31], [32]. Amer et al.[28] proposed a Multimodal Discriminative CRBMs (MMDCRBMs) model based on a Conditional RBMs (an extension of the RBM). Its training process is composed of training each modality using labeled data and training a fusion layer. For multi-modality deep learning, Bu et al.[33] developed a supervised 3D feature learning framework in which a RBM is used to mine the deep correlations of different modalities. Cheng et al.[34] presented a novel duplex metric learning (DML) framework for feature learning and image classification. The main task of DML is to learn an effective hidden layer feature of a discriminative stacked autoencoder (DSAE). In the feature space of the DSAE, similar and dissimilar samples are mapped close to each other and further apart, respectively. This framework is the most related work to our study, but it belongs to supervised feature learning with a DSAE by layer-wisely imposing metric learning method and it is applied to image classification tasks.

However, supervision information, e.g., labels, is scarce and

it is expensive to obtain more labels in many applications. So, some works[35], [36], [37], [22] explored semi-supervised feature learning which only needs a small number of labels. Chu et al.[22] presented a pcGRBM model by fusing pairwise constraints into the reconstructed visible layer for clustering tasks. To mitigate the burden of annotation, Yesilbek and Sezgin[36] applied self-learning methods to build a system that can learn from large amounts of unlabeled data and few labeled examples for sketch recognition. The systems perform self-learning by extending a small labeled set with new examples which are extracted from unlabeled sketches. Chen et al.[37] developed a deep sparse auto-encoder network with supervised fine-tuning and unsupervised layer-wise self-learning for fault identification. As a whole, these works belong to semi-supervised learning methods.

Many unsupervised feature learning approaches based on the RBMs have been proposed by previous researches[38], [39], [40], [41], [42], [43], [44], [45], [13], [46]. Chopra and Yadav[44] presented a unique technique to extract fault feature from the noisy acoustic signal by an unsupervised RBM. Zhang et al.[45] proposed unsupervised feature learning based on recursive autoencoders network (RAE) for image classification. They used the spectral and spatial information from original data to produce high-level features. Chen et al.[13] illustrated a new graph regularized RBM (GraphRBM) to extract hidden layer representations for unsupervised clustering and classification problem. Meanwhile, they have considered the manifold structure of the original data. Xie et al.[46] showed a novel approach to optimize RBM pre-training by capturing principal component directions of the input with principal component analysis. Al-Dmour and Al-Ani[47] proposed a fully-automatic segmentation algorithm in which a neural network (NN) model is used to extract the features of the brain tissue image and is trained using clustering labels produced by three clustering algorithms. The obtained classes are combined by majority voting. The study is closely related to our work, but our encoding framework based on RBMs is guided by self-learning local supervisions which stem from unsupervised clustering algorithms and unanimous voting strategy are integrated into the CD learning of RBMs to constrict and disperse the distribution of the hidden layer features and reconstructed hidden layer features. Stewart and Ermon[48] presented a new technique to supervise NN by prior domain knowledge for computer vision tasks. It is a related work to our study. However, their work faces to a convolutional neural network (CNN) and requires large amounts of prior domain knowledge and how to encode prior knowledge into loss functions of a CNN is a new challenge.

Two existing voting strategies are often used to supervised learning in previous researches. One is the max-voting scheme. For example, Azimi et al.[49] developed a deep learning method for low carbon steel microstructural classification via fully CNN (FCNN) accompanied by a max-voting scheme. The other is the majority voting scheme. For example, Seera et al.[50] applied a recurrent neural network (RNN) to extract features from the Transcranial Doppler (TCD) signals for classification tasks. This work proposed an ensemble RNN model in which the majority voting scheme is used to combine

the single RNN predictions. Recently various voting classifiers using majority voting have been proposed to enhance the performance of the classification[51], [52], [53], [54], [55], [56].

In our following work, we explore unsupervised feature learning based on RBMs to constrict and disperse hidden layer feature distribution for clustering tasks.

III. THEORETICAL BACKGROUND

A. Restricted Boltzmann Machine

A RBM[10] consists of two-layer structure: a visible layer and a hidden layer with stochastic binary units via symmetrically weighted connections. It has no any interior-layer connections both between the visible layer units and between the hidden layer units. An energy function of a joint distribution of the visible layer and hidden layer units takes the form:

$$E(\mathbf{v}, \mathbf{h}) = - \sum_{i \in \text{visibles}} a_i v_i - \sum_{j \in \text{hidens}} b_j h_j - \sum_{i,j} v_i h_j w_{ij}, \quad (1)$$

where \mathbf{v} is the visible layer vectors and v_i is its the binary states of visible unit i , \mathbf{h} is the hidden layer vectors and h_j is its the binary states of hidden unit j , a_i and b_j are the biases of visible layer and hidden layer respectively, w_{ij} is the symmetric connection weight between v_i and h_j .

The conditional probability distributions of hidden layer and visible layer units of the RBM are given by:

$$p(h_j = 1 | \mathbf{v}) = \sigma(b_j + \sum_i v_i w_{ij}) \quad (2)$$

and

$$p(v_i = 1 | \mathbf{h}) = \sigma(a_i + \sum_j h_j w_{ij}), \quad (3)$$

where σ is the sigmoid function.

B. Linear Visible Units

The classical RBM was designed with binary units for both the hidden and visible layers[12]. For training real-valued data, the visible layer of RBM consists of Gaussian linear units and the hidden layer of RBM is still binary units. The energy function of RBM with Gaussian linear visible units takes the form:

$$E(\mathbf{v}, \mathbf{h}) = - \sum_{i \in \text{visibles}} \frac{v_i - a_i}{2\sigma_i^2} - \sum_{j \in \text{hidens}} b_j h_j - \sum_{i,j} \frac{v_i}{\sigma_i} h_j w_{ij}, \quad (4)$$

where σ_i is the standard deviation of visible unit i with Gaussian noise. In the visible layer, the conditional probability is defined by:

$$p(\mathbf{v} | \mathbf{h}) = \mathcal{N}(\sum \mathbf{h} \mathbf{W}^T + \mathbf{a}, \sigma^2), \quad (5)$$

where $\mathcal{N}(\cdot)$ represents gaussian density ($\mu = \sum \mathbf{h} \mathbf{W}^T + \mathbf{a}$). The update rules of the parameters become simple when the linear visible units have unit variance of Gaussian noise. This type of noise-free visible units are used for one of the proposed models (slsGRBM) based on our novel framework described later. Then, the reconstructed values of Gaussian linear visible units are equal to their top-down input values from the binary hidden units plus their bias.

C. Contrastive Divergence Learning

To learn the parameters of symmetric connection weight by Maximum-likelihood learning, the update rule is given by:

$$\Delta w_{ij} = \varepsilon(\langle v_i h_j \rangle_{data} - \langle v_i h_j \rangle_{model}), \quad (6)$$

where ε is a learning rate. But it is very slow to obtain unbiased sample of $\langle v_i h_j \rangle_{model}$.

So, a faster learning algorithm[12] was proposed by applying approximating the gradient of CD. Then the change of symmetric connection weight with one step CD is given by:

$$\Delta w_{ij} = \varepsilon(\langle v_i h_j \rangle_{data} - \langle v_i h_j \rangle_{recon}), \quad (7)$$

where the hidden layer units are driven by visible data, $\langle v_i h_j \rangle_{data}$ is the multiple that visible layer unit i and hidden layer unit j are on together, $\langle v_i h_j \rangle_{recon}$ represents the corresponding reconstructions. Similarly, the changes of biases a_i and b_j with one step CD are given by:

$$\Delta a_i = \varepsilon(\langle v_i \rangle_{data} - \langle v_i \rangle_{recon}) \quad (8)$$

and

$$\Delta b_j = \varepsilon(\langle h_j \rangle_{data} - \langle h_j \rangle_{recon}). \quad (9)$$

So, the update rules of all parameters take the form

$$w_{ij}^{(\tau+1)} = w_{ij}^{(\tau)} + \varepsilon(\langle v_i h_j \rangle_{data} - \langle v_i h_j \rangle_{recon}), \quad (10)$$

$$a_i^{(\tau+1)} = a_i^{(\tau)} + \varepsilon(\langle v_i \rangle_{data} - \langle v_i \rangle_{recon}) \quad (11)$$

and

$$b_j^{(\tau+1)} = b_j^{(\tau)} + \varepsilon(\langle h_j \rangle_{data} - \langle h_j \rangle_{recon}). \quad (12)$$

The learning efficiency can be obviously improved by the CD learning.

IV. SELF-LEARNING LOCAL SUPERVISION ENCODING FRAMEWORK AND LEARNING ALGORITHMS

In this section, we present a novel self-learning local supervision encoding framework based on RBMs, in which the self-learning local supervisions from visible layer are integrated into the CD learning of RBMs to constrict and disperse the distribution of the hidden layer features. In the framework, we use sigmoid transformation to obtain hidden layer and reconstructed hidden layer features from visible layer and reconstructed visible layer units during sampling procedure. The self-learning local supervisions contain local credible clusters which stem from different unsupervised learning and unanimous voting strategy. For the same local clusters, the hidden features of the input and reconstructed data of the framework tends to constrict together. Furthermore, the center of different local clusters of hidden layer tends to disperse in the encoding process. The structure of the framework is shown in Fig. 1.

TABLE I
LIST OF SYMBOLS.

Notation	Definition
V_{data}	Visible layer data set
H_{data}	Hidden layer feature set
V_{recon}	Reconstructed visible layer set
H_{recon}	Hidden layer feature of reconstructed visible layer set
$\mathbf{v}_s, \mathbf{v}_t$	Visible layer row vector
$\mathbf{h}_s, \mathbf{h}_t$	Hidden layer feature row vector
$\tilde{\mathbf{v}}_s, \tilde{\mathbf{v}}_t$	Reconstructed visible layer row vector
$\tilde{\mathbf{h}}_s, \tilde{\mathbf{h}}_t$	Hidden layer feature row vector of reconstructed data
\tilde{V}_k	All vectors of $\tilde{V}_k \subset V_{recon}$ belong to the same cluster.
\tilde{V}_k	All vectors of $\tilde{V}_k \subset V_{recon}$ belong to the same cluster.
\tilde{H}_k	All vectors of $\tilde{H}_k \subset H_{recon}$ belong to the same cluster.
\tilde{H}_k	All vectors of $\tilde{H}_k \subset H_{recon}$ belong to the same cluster.
\mathbf{C}_k	The center of cluster H_k
$\tilde{\mathbf{C}}_k$	The center of cluster \tilde{H}_k
\mathbf{O}_k	The center of cluster V_k
$\tilde{\mathbf{O}}_k$	The center of cluster \tilde{V}_k

A. The Framework

Suppose that $V_{data} = \{\mathbf{v}_1, \mathbf{v}_2, \dots, \mathbf{v}_N\}$ is the original data set. $H_{data} = \{\mathbf{h}_1, \mathbf{h}_2, \dots, \mathbf{h}_N\}$ is the hidden layer feature set. $V_{recon} = \{\tilde{\mathbf{v}}_1, \tilde{\mathbf{v}}_2, \dots, \tilde{\mathbf{v}}_P\}$ is the reconstructed visible layer data set. $H_{recon} = \{\tilde{\mathbf{h}}_1, \tilde{\mathbf{h}}_2, \dots, \tilde{\mathbf{h}}_P\}$ is the hidden features set of reconstructed data. Let V_1, V_2, \dots, V_K be K local clusters of visible layer set V_{data} , $H_i (i = 1, 2, \dots, K)$ are local clusters mapped of $V_i (i = 1, 2, \dots, K)$, respectively. Similarly, $\tilde{V}_1, \tilde{V}_2, \dots, \tilde{V}_K$ are K local clusters of reconstructed visible layer set V_{recon} , $\tilde{H}_i (i = 1, 2, \dots, K)$ are K local clusters mapped of $\tilde{V}_i (i = 1, 2, \dots, K)$, respectively. We use the gradient descent method to obtain approximate optimal parameters of the framework. It is expensive to compute the gradient of the log probability of RBMs. However, Karakida et al.[27] demonstrated that \mathbf{CD}_1 learning is simpler than ML learning in RBMs. Therefore, we apply the \mathbf{CD}_1 learning method to obtain an approximation of the log probability gradient of RBMs.

Then the objective function takes the form:

$$\begin{aligned} F(\theta, V_{data}) = & \\ & - \frac{\eta}{N} \sum_{\mathbf{v} \in V_{data}} \log p(\mathbf{v}; \theta) + \left(\frac{1-\eta}{N_h} \sum_{k=1}^K \sum_{\mathbf{h}_s, \mathbf{h}_t \in H_k} \|\mathbf{h}_s - \mathbf{h}_t\|^2 \right. \\ & - \frac{1-\eta}{N_C} \sum_{p=1}^{K-1} \sum_{q=p+1}^K \|\mathbf{C}_p - \mathbf{C}_q\|^2 \left. + \left(\frac{1-\eta}{N_h} \sum_{k=1}^K \sum_{\tilde{\mathbf{h}}_s, \tilde{\mathbf{h}}_t \in \tilde{H}_k} \right. \right. \\ & \left. \left. \|\tilde{\mathbf{h}}_s - \tilde{\mathbf{h}}_t\|^2 - \frac{1-\eta}{N_C} \sum_{p=1}^{K-1} \sum_{q=p+1}^K \|\tilde{\mathbf{C}}_p - \tilde{\mathbf{C}}_q\|^2 \right) \right), \end{aligned} \quad (13)$$

where $\theta = \{\mathbf{a}, \mathbf{b}, \mathbf{W}\}$ are the model parameters, $\eta \in (0, 1)$ is a scale coefficient, N_h is the cardinality of $H_k (k = 1, 2, \dots, K)$, $N_C = \frac{K(K-1)}{2}$ is the number of pairwise cluster center, $\frac{\eta}{N} \sum_{\mathbf{v} \in V_{data}} \log p(\mathbf{v}; \theta)$ is the average of the log-likelihood and $\|\cdot\|^2$ is the square of 2-norm. For the same local cluster, the hidden layer features and the reconstructed hidden layer features tend to constrict together in the training procedure. Meanwhile, the center of different local clusters tends to disperse in the hidden layer and the reconstructed hidden layer.

Let

$$L_{data}(\theta) = \frac{1}{N_h} \sum_{k=1}^K \sum_{\mathbf{h}_s, \mathbf{h}_t \in \mathbb{H}_k} \|\mathbf{h}_s - \mathbf{h}_t\|^2 - \frac{1}{N_C} \sum_{p=1}^{K-1} \sum_{q=p+1}^K \|\mathbf{C}_p - \mathbf{C}_q\|^2 \quad (14)$$

and

$$L_{recon}(\theta) = \frac{1}{N_h} \sum_{k=1}^K \sum_{\tilde{\mathbf{h}}_s, \tilde{\mathbf{h}}_t \in \tilde{\mathbb{H}}_k} \|\tilde{\mathbf{h}}_s - \tilde{\mathbf{h}}_t\|^2 - \frac{1}{N_C} \sum_{p=1}^{K-1} \sum_{q=p+1}^K \|\tilde{\mathbf{C}}_p - \tilde{\mathbf{C}}_q\|^2. \quad (15)$$

Then the objective function is as follows:

$$F(\theta, \nabla_{data}) = -\frac{\eta}{N} \sum_{\mathbf{v}_i \in \nabla_{data}} \log p(\mathbf{v}_i; \theta) + (1 - \eta) [L_{data}(\theta) + L_{recon}(\theta)]. \quad (16)$$

The next problems are how to get the gradients of $L_{data}(\theta)$ and $L_{recon}(\theta)$. Firstly, we compute the gradients of L_{data} as follows. Because $L_{data}(\theta)$ has another equivalent form:

$$L_{data}(\theta) = \frac{1}{N_h} \sum_{k=1}^K \sum_{\mathbf{h}_s, \mathbf{h}_t \in \mathbb{H}_k} (\mathbf{h}_s - \mathbf{h}_t)(\mathbf{h}_s - \mathbf{h}_t)^T - \frac{1}{N_C} \sum_{p=1}^{K-1} \sum_{q=p+1}^K (\mathbf{C}_p - \mathbf{C}_q)(\mathbf{C}_p - \mathbf{C}_q)^T. \quad (17)$$

Then we can obtain:

$$\begin{aligned} \frac{\partial L_{data}(\theta)}{\partial w_{ij}} &= \frac{1}{N_h} \left[\sum_{k=1}^K \sum_{\mathbf{h}_s, \mathbf{h}_t \in \mathbb{H}_k} (\mathbf{h}_s - \mathbf{h}_t) \frac{\partial (\mathbf{h}_s - \mathbf{h}_t)^T}{\partial w_{ij}} + \sum_{k=1}^K \sum_{\mathbf{h}_s, \mathbf{h}_t \in \mathbb{H}_k} \frac{\partial (\mathbf{h}_s - \mathbf{h}_t)}{\partial w_{ij}} (\mathbf{h}_s - \mathbf{h}_t)^T \right] - \\ &\frac{1}{N_C} \left[\sum_{p=1}^{K-1} \sum_{q=p+1}^K (\mathbf{C}_p - \mathbf{C}_q) \frac{\partial (\mathbf{C}_p - \mathbf{C}_q)^T}{\partial w_{ij}} + \sum_{p=1}^{K-1} \sum_{q=p+1}^K \frac{\partial (\mathbf{C}_p - \mathbf{C}_q)}{\partial w_{ij}} (\mathbf{C}_p - \mathbf{C}_q)^T \right]. \end{aligned} \quad (18)$$

From above result, we can see that the following task is how to compute $\frac{\partial (\mathbf{h}_s - \mathbf{h}_t)^T}{\partial w_{ij}}$, $\frac{\partial (\mathbf{h}_s - \mathbf{h}_t)}{\partial w_{ij}}$, $\frac{\partial (\mathbf{C}_p - \mathbf{C}_q)^T}{\partial w_{ij}}$ and $\frac{\partial (\mathbf{C}_p - \mathbf{C}_q)}{\partial w_{ij}}$. Next, all of them are solved separately.

$$\begin{aligned} \frac{\partial (\mathbf{h}_s - \mathbf{h}_t)^T}{\partial w_{ij}} &= \left(\frac{\partial \mathbf{h}_s}{\partial w_{ij}} - \frac{\partial \mathbf{h}_t}{\partial w_{ij}} \right)^T \\ &= \left[\frac{\partial (\sigma \mathbf{b} + \mathbf{v}_s \mathbf{W})}{\partial w_{ij}} - \frac{\partial (\sigma \mathbf{b} + \mathbf{v}_t \mathbf{W})}{\partial w_{ij}} \right]^T. \end{aligned} \quad (19)$$

Obviously, $\sigma(\mathbf{b} + \mathbf{v}_s \mathbf{W})$ is a row vector, all components of which are independent of w_{ij} except j component. So,

$$\frac{\partial \sigma(\mathbf{b} + \mathbf{v}_s \mathbf{W})}{\partial w_{ij}} = \left(\underbrace{0, \dots, 0}_{j-1}, \frac{\partial \sigma(b_j + \sum_{i=1}^n v_{si} w_{ij})}{\partial w_{ij}}, \underbrace{0, \dots, 0}_{n-j} \right). \quad (20)$$

Because $\frac{\partial \sigma(b_j + \sum_{i=1}^n v_{si} w_{ij})}{\partial w_{ij}} = h_{sj}(1 - h_{sj})v_{si}$, the final result of $\frac{\partial \sigma(\mathbf{b} + \mathbf{v}_s \mathbf{W})}{\partial w_{ij}}$ has an expression as follows:

$$\frac{\partial \sigma(\mathbf{b} + \mathbf{v}_s \mathbf{W})}{\partial w_{ij}} = \left(\underbrace{0, \dots, 0}_{j-1}, h_{sj}(1 - h_{sj})v_{si}, \underbrace{0, \dots, 0}_{n-j} \right). \quad (21)$$

Similarly, the expression of final result of $\frac{\partial \sigma(\mathbf{b} + \mathbf{v}_t \mathbf{W})}{\partial w_{ij}}$ is as follows:

$$\frac{\partial \sigma(\mathbf{b} + \mathbf{v}_t \mathbf{W})}{\partial w_{ij}} = \left(\underbrace{0, \dots, 0}_{j-1}, h_{tj}(1 - h_{tj})v_{ti}, \underbrace{0, \dots, 0}_{n-j} \right). \quad (22)$$

Then, the final result of $\frac{\partial (\mathbf{h}_s - \mathbf{h}_t)^T}{\partial w_{ij}}$ is a column vector:

$$\begin{aligned} \frac{\partial (\mathbf{h}_s - \mathbf{h}_t)^T}{\partial w_{ij}} &= \left(\underbrace{0, \dots, 0}_{j-1}, h_{sj}(1 - h_{sj})v_{si} - h_{tj}(1 - h_{tj})v_{ti}, \underbrace{0, \dots, 0}_{n-j} \right)^T. \end{aligned} \quad (23)$$

Similarly,

$$\frac{\partial (\mathbf{h}_s - \mathbf{h}_t)}{\partial w_{ij}} = \left(\underbrace{0, \dots, 0}_{j-1}, h_{sj}(1 - h_{sj})v_{si} - h_{tj}(1 - h_{tj})v_{ti}, \underbrace{0, \dots, 0}_{n-j} \right), \quad (24)$$

$$\begin{aligned} \frac{\partial (\mathbf{C}_p - \mathbf{C}_q)^T}{\partial w_{ij}} &= \left(\underbrace{0, \dots, 0}_{j-1}, C_{pj}(1 - C_{pj})O_{pi} - C_{qj}(1 - C_{qj})O_{qi}, \underbrace{0, \dots, 0}_{n-j} \right)^T \end{aligned} \quad (25)$$

and

$$\frac{\partial (\mathbf{C}_p - \mathbf{C}_q)}{\partial w_{ij}} = \left(\underbrace{0, \dots, 0}_{j-1}, C_{pj}(1 - C_{pj})O_{pi} - C_{qj}(1 - C_{qj})O_{qi}, \underbrace{0, \dots, 0}_{n-j} \right). \quad (26)$$

Eq. (23), Eq. (24), Eq. (25) and Eq. (26) are substituted in Eq. (18). Then we have

$$\begin{aligned} \frac{\partial L_{data}(\theta)}{\partial w_{ij}} &= \frac{2}{N_h} \sum_{k=1}^K \sum_{\mathbf{h}_s, \mathbf{h}_t \in \mathbb{H}_k} (h_{sj} - h_{tj}) \left[h_{sj}(1 - h_{sj})v_{si} - h_{tj}(1 - h_{tj})v_{ti} \right] \\ &- \frac{2}{N_C} \sum_{p=1}^{K-1} \sum_{q=p+1}^K (C_{pj} - C_{qj}) \left[C_{pj}(1 - C_{pj})O_{pi} - C_{qj}(1 - C_{qj})O_{qi} \right]. \end{aligned} \quad (27)$$

Using above same solution, we can obtain:

$$\begin{aligned} \frac{\partial L_{recon}(\theta)}{\partial w_{ij}} = & \frac{2}{N_h} \sum_{k=1}^K \sum_{\tilde{\mathbf{h}}_s, \tilde{\mathbf{h}}_t \in \tilde{\mathbb{H}}_k} (\tilde{h}_{sj} - \tilde{h}_{tj}) \left[\tilde{h}_{sj}(1 - \tilde{h}_{sj})\tilde{v}_{si} - \tilde{h}_{tj}(1 - \tilde{h}_{tj})\tilde{v}_{ti} \right] \\ & - \frac{2}{N_C} \sum_{p=1}^{K-1} \sum_{q=p+1}^K (\tilde{C}_{pj} - \tilde{C}_{qj}) \left[\tilde{C}_{pj}(1 - \tilde{C}_{pj})\tilde{o}_{pi} - \right. \\ & \left. \tilde{C}_{qj}(1 - \tilde{C}_{qj})\tilde{o}_{qi} \right]. \end{aligned} \quad (28)$$

The following task is how to obtain $\frac{\partial L_{recon}(\theta)}{\partial b_j}$ and

$\frac{\partial L_{recon}(\theta)}{\partial b_j}$. Because $\frac{\partial \sigma(b_j + \sum_{i=1}^n v_{si} w_{ij})}{\partial b_j} = h_{sj}(1 - h_{sj})$ and $\frac{\partial \sigma(b_j + \sum_{i=1}^n v_{ti} w_{ij})}{\partial b_j} = h_{tj}(1 - h_{tj})$, the final result of $\frac{\partial \sigma(\mathbf{b} + \mathbf{v}_s \mathbf{W})}{\partial b_j}$ and $\frac{\partial \sigma(\mathbf{b} + \mathbf{v}_t \mathbf{W})}{\partial b_j}$ have expressions as follows:

$$\frac{\partial \sigma(\mathbf{b} + \mathbf{v}_s \mathbf{W})}{\partial b_j} = (\underbrace{0, \dots, 0}_{j-1}, h_{sj}(1 - h_{sj}), \underbrace{0, \dots, 0}_{n-j}) \quad (29)$$

and

$$\frac{\partial \sigma(\mathbf{b} + \mathbf{v}_t \mathbf{W})}{\partial b_j} = (\underbrace{0, \dots, 0}_{j-1}, h_{tj}(1 - h_{tj}), \underbrace{0, \dots, 0}_{n-j}). \quad (30)$$

So, the final result of $\frac{\partial L_{data}(\theta)}{\partial b_j}$ is as follows.

$$\begin{aligned} \frac{\partial L_{data}(\theta)}{\partial b_j} = & \frac{2}{N_h} \sum_{k=1}^K \sum_{\mathbf{h}_s, \mathbf{h}_t \in \mathbb{H}_k} (h_{sj} - h_{tj}) \left[h_{sj}(1 - h_{sj}) - h_{tj}(1 - h_{tj}) \right] \\ & - \frac{2}{N_C} \sum_{p=1}^{K-1} \sum_{q=p+1}^K (C_{pj} - C_{qj}) \left[C_{pj}(1 - C_{pj}) - \right. \\ & \left. C_{qj}(1 - C_{qj}) \right]. \end{aligned} \quad (31)$$

Similarly, the expression of $\frac{\partial L_{recon}(\theta)}{\partial b_j}$ is as follows.

$$\begin{aligned} \frac{\partial L_{recon}(\theta)}{\partial b_j} = & \frac{2}{N_h} \sum_{k=1}^K \sum_{\tilde{\mathbf{h}}_s, \tilde{\mathbf{h}}_t \in \tilde{\mathbb{H}}_k} (\tilde{h}_{sj} - \tilde{h}_{tj}) \left[\tilde{h}_{sj}(1 - \tilde{h}_{sj}) - \tilde{h}_{tj}(1 - \tilde{h}_{tj}) \right] \\ & - \frac{2}{N_C} \sum_{p=1}^{K-1} \sum_{q=p+1}^K (\tilde{C}_{pj} - \tilde{C}_{qj}) \left[\tilde{C}_{pj}(1 - \tilde{C}_{pj}) - \right. \\ & \left. \tilde{C}_{qj}(1 - \tilde{C}_{qj}) \right]. \end{aligned} \quad (32)$$

Because $\frac{\partial \sigma(b_j + \sum_{i=1}^n v_{si} w_{ij})}{\partial a_i} = 0$ and $\frac{\partial \sigma(b_j + \sum_{i=1}^n v_{ti} w_{ij})}{\partial a_i} = 0$, the final result of $\frac{\partial \sigma(\mathbf{b} + \mathbf{v}_s \mathbf{W})}{\partial a_i} = \mathbf{0}$ and $\frac{\partial \sigma(\mathbf{b} + \mathbf{v}_t \mathbf{W})}{\partial a_i} = \mathbf{0}$. Then we can obtain: $\frac{\partial L_{data}(\theta)}{\partial a_i} = 0$, $\frac{\partial L_{recon}(\theta)}{\partial a_i} = 0$.

Finally, following the \mathbf{CD}_1 learning and the gradient of the L_{data} and L_{recon} , the update rules of the symmetric connection weight take the form

$$\begin{aligned} w_{ij}^{(\tau+1)} = & w_{ij}^{(\tau)} + \eta \varepsilon (\langle v_i h_j \rangle_{data} - \langle v_i h_j \rangle_{recon}) + (1 - \eta) \\ & \left\{ \frac{2}{N_h} \sum_{k=1}^K \sum_{\mathbf{h}_s, \mathbf{h}_t \in \mathbb{H}_k} (h_{sj} - h_{tj}) \left[h_{sj}(1 - h_{sj})v_{si} - h_{tj}(1 - h_{tj})v_{ti} \right] \right. \\ & - \frac{2}{N_C} \sum_{p=1}^{K-1} \sum_{q=p+1}^K (C_{pj} - C_{qj}) \left[C_{pj}(1 - C_{pj})O_{pi} - \right. \\ & \left. \left. C_{qj}(1 - C_{qj})O_{qi} \right] \right\} + (1 - \eta) \\ & \left\{ \frac{2}{N_h} \sum_{k=1}^K \sum_{\tilde{\mathbf{h}}_s, \tilde{\mathbf{h}}_t \in \tilde{\mathbb{H}}_k} (\tilde{h}_{sj} - \tilde{h}_{tj}) \left[\tilde{h}_{sj}(1 - \tilde{h}_{sj})\tilde{v}_{si} - \tilde{h}_{tj}(1 - \tilde{h}_{tj})\tilde{v}_{ti} \right] \right. \\ & - \frac{2}{N_C} \sum_{p=1}^{K-1} \sum_{q=p+1}^K (\tilde{C}_{pj} - \tilde{C}_{qj}) \left[\tilde{C}_{pj}(1 - \tilde{C}_{pj})\tilde{o}_{pi} - \right. \\ & \left. \left. \tilde{C}_{qj}(1 - \tilde{C}_{qj})\tilde{o}_{qi} \right] \right\}. \end{aligned} \quad (33)$$

The update rules of biases b_j take the form

$$\begin{aligned} b_j^{(\tau+1)} = & b_j^{(\tau)} + \eta \varepsilon (\langle h_j \rangle_{data} - \langle h_j \rangle_{recon}) + (1 - \eta) \\ & \left\{ \frac{2}{N_h} \sum_{k=1}^K \sum_{\mathbf{h}_s, \mathbf{h}_t \in \mathbb{H}_k} (h_{sj} - h_{tj}) \left[h_{sj}(1 - h_{sj}) - h_{tj}(1 - h_{tj}) \right] \right. \\ & - \frac{2}{N_C} \sum_{p=1}^{K-1} \sum_{q=p+1}^K (C_{pj} - C_{qj}) \left[C_{pj}(1 - C_{pj}) - \right. \\ & \left. \left. C_{qj}(1 - C_{qj}) \right] \right\} + (1 - \eta) \\ & \left\{ \frac{2}{N_h} \sum_{k=1}^K \sum_{\tilde{\mathbf{h}}_s, \tilde{\mathbf{h}}_t \in \tilde{\mathbb{H}}_k} (\tilde{h}_{sj} - \tilde{h}_{tj}) \left[\tilde{h}_{sj}(1 - \tilde{h}_{sj}) - \tilde{h}_{tj}(1 - \tilde{h}_{tj}) \right] \right. \\ & - \frac{2}{N_C} \sum_{p=1}^{K-1} \sum_{q=p+1}^K (\tilde{C}_{pj} - \tilde{C}_{qj}) \left[\tilde{C}_{pj}(1 - \tilde{C}_{pj}) - \right. \\ & \left. \left. \tilde{C}_{qj}(1 - \tilde{C}_{qj}) \right] \right\} \end{aligned} \quad (34)$$

and the update rules of biases a_i take the form

$$a_i^{(\tau+1)} = a_i^{(\tau)} + \eta \varepsilon (\langle v_i \rangle_{data} - \langle v_i \rangle_{recon}). \quad (35)$$

Under such a framework, we present two instantiation models with two different visible layer reconstruction. One is self-learning local supervision GRBM (slsGRBM) model with Gaussian linear visible units and binary hidden units using linear transformation for visible layer reconstruction. The other is self-learning local supervision RBM (slsRBM) model with with binary visible and hidden units using sigmoid transformation for visible layer reconstruction.

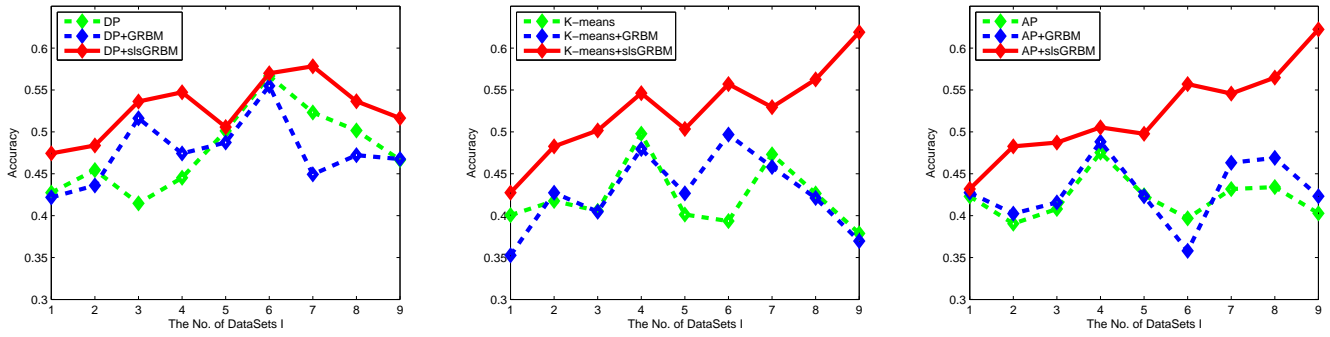


Fig. 2. Comparison of the proposed algorithms (DP+slsGRBM, K-means+slsGRBM and AP+slsGRBM) and contrastive algorithms using the evaluating indicator of the accuracy. The X axis indicates the serial number of data sets I.

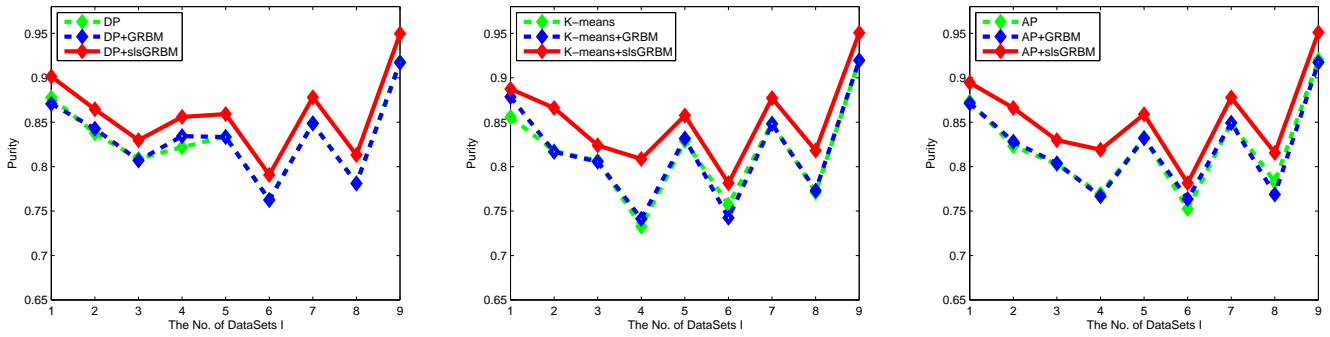


Fig. 3. Comparison of the proposed algorithms (DP+slsGRBM, K-means+slsGRBM and AP+slsGRBM) and contrastive algorithms using the evaluating indicator of the purity. The X axis indicates the serial number of data sets I.

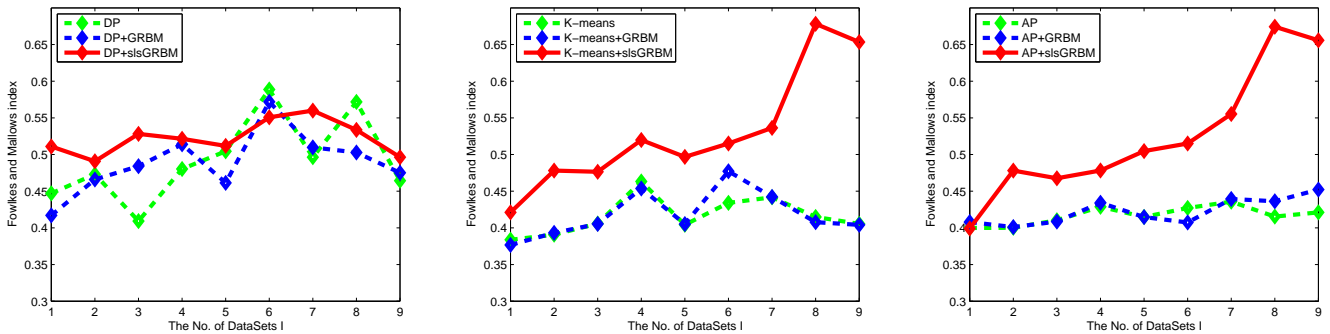


Fig. 4. Comparison of the proposed algorithms (DP+slsGRBM, K-means+slsGRBM and AP+slsGRBM) and contrastive algorithms using the evaluating indicator of the Fowlkes and Mallows Index. The X axis indicates the serial number of data sets I.

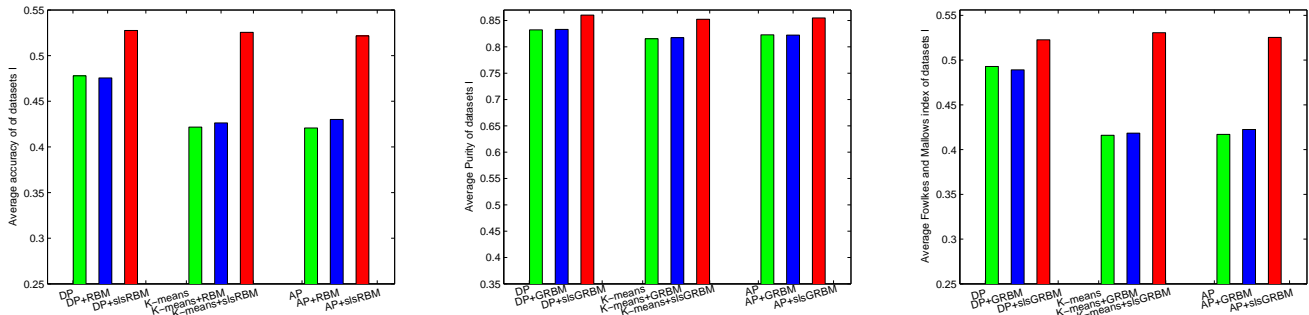


Fig. 5. Comparison of the proposed algorithms (DP+slsGRBM, K-means+slsGRBM and AP+slsGRBM) and contrastive algorithms using average accuracy, purity and Fowlkes and Mallows Index (datasets I). The X axis indicates the name of contrastive algorithms.

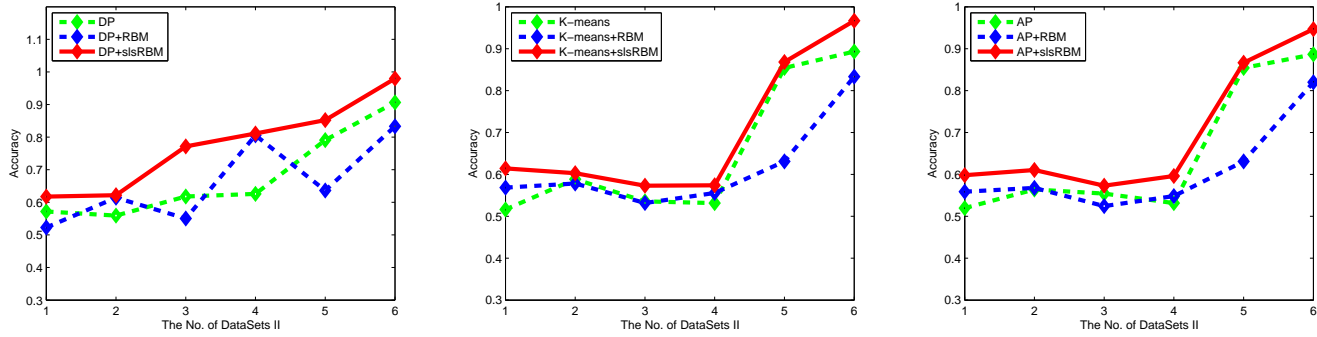


Fig. 6. Comparison of the proposed algorithms (DP+slsRBM, K-means+slsRBM and AP+slsRBM) and contrastive algorithms using the evaluating indicator of the accuracy. The X axis indicates the serial number of data sets II.

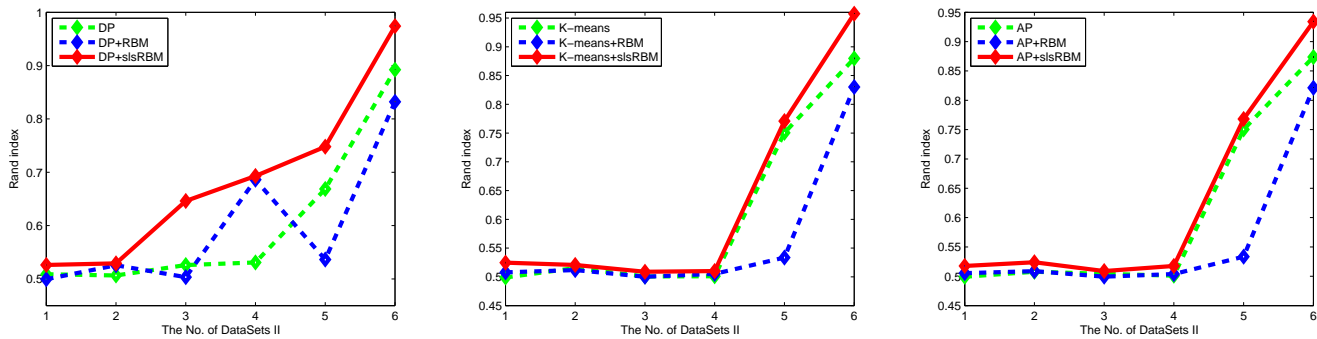


Fig. 7. Comparison of the proposed algorithms (DP+slsRBM, K-means+slsRBM and AP+slsRBM) and contrastive algorithms using the evaluating indicator of the rand index. The X axis indicates the serial number of data sets II.

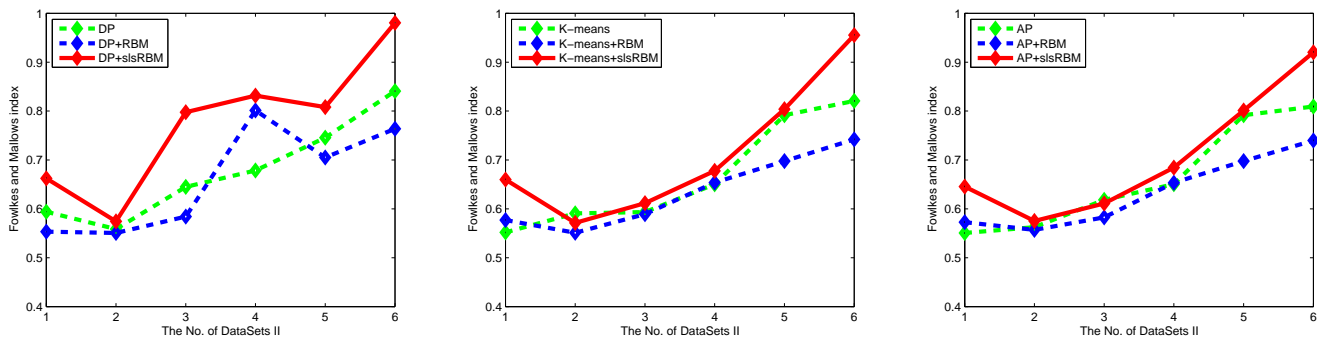


Fig. 8. Comparison of the proposed algorithms (DP+slsRBM, K-means+slsRBM and AP+slsRBM) and contrastive algorithms using the evaluating indicator of the FMI. The X axis indicates the serial number of data sets II.

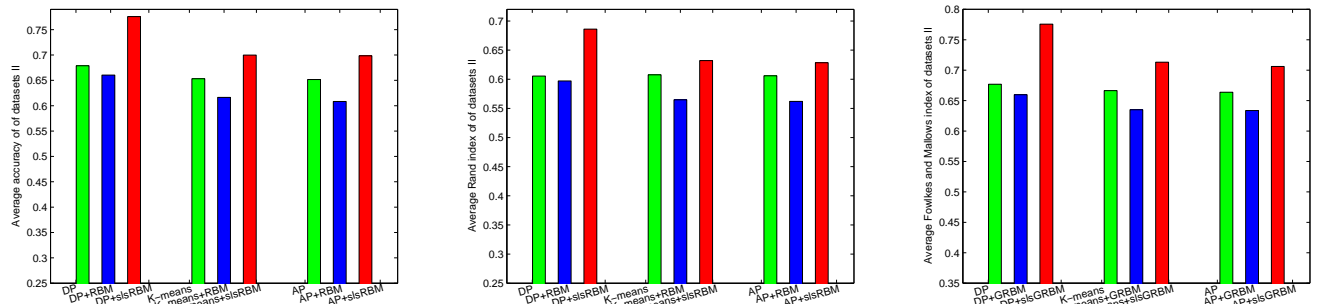


Fig. 9. Comparison of the proposed algorithms (DP+slsRBM, K-means+slsRBM and AP+slsRBM) and contrastive algorithms using average accuracy, Rand index and FMI (datasets II). The X axis indicates the name of contrastive algorithms.

TABLE II
SUMMARY OF THE EXPERIMENT DATASETS I.

No.	Dataset	classes	Instances	feature
1	Book (BO)	3	896	892
2	Water (WA)	3	922	899
3	Weddingring (WR)	3	897	899
4	Birthdaycake (BC)	3	932	892
5	Vegetable (VE)	3	872	899
6	Ambulances (AM)	3	930	892
7	Vista (VI)	3	799	899
8	Wallpaper (WP)	3	919	899
9	Voituretuning (VT)	3	879	899

TABLE III
SUMMARY OF THE EXPERIMENT DATASETS II (UCI).

No.	Dataset	classes	Instances	feature
1	Haberman's Survival (HS)	2	306	3
2	QSAR biodegradation (QB)	2	1055	41
3	SPECT Heart (SH)	2	267	22
4	Simulation Crashes (SC)	2	540	18
5	Breast Cancer Wisconsin (BCW)	2	569	32
6	Iris (IR)	3	150	4

V. EXPERIMENT RESULTS AND DISCUSSION

A. Experimental Settings

The experimental evaluations are performed by unsupervised clustering tasks. Using the hidden layer features of the proposed sIsGRBM model as the input of three unsupervised clustering algorithms, e.g., density peaks (DP)[57], K-means[58] and affinity propagation (AP)[59]. We design three unsupervised clustering algorithms are termed as DP+sIsGRBM, K-means+sIsGRBM and AP+sIsGRBM, respectively. Similarly, another three unsupervised clustering algorithms termed as DP+sIsRBM, K-means+sIsRBM and AP+sIsRBM based on the proposed sIsRBM model, respectively.

1) *Datasets*: We use the Microsoft Research Asia Multimedia (MSRA-MM)2.0 real-valued data set[60] for our evaluations of the proposed sIsGRBM model. The summary of the experiment datasets is shown in Table II. Three datasets Book (Bo), Birthdaycake (BC) and Ambulances (AM) contain 896, 932 and 930 instances, respectively. All of them have 892 features. For the other six datasets Water (WA), Weddingring (WR), Vegetable (VE), Vista (VI), Wallpaper (WP) and Voituretuning (VT) have 899 features. They contain 922, 897, 872, 799, 919 and 879 instances, respectively. We also use six UCI data sets for the proposed sIsRBM model. The summary of them is shown in Table III. The Haberman's Survival (HS) data set contains 306 instances and three features. The QSAR biodegradation (QB) data set contains 1055 instances and 41 features. The SPECT Heart (SH) data set contains 267 instances and 22 features. The Simulation Crashes (SC) data set contains 540 instances and 18 features. The Breast Cancer Wisconsin (BCW) data set contains 569 instances and 32 features. The last one data set is Iris (IR), which has 150 instances and 4 features.

2) *Self-learning Local Supervision*: We use three unsupervised clustering algorithms, e.g., DP, K-means and AP to obtain three cluster divisions. These divisions originate un-

pervised learning, so we call them self-learning supervision. In order to obtain more reliable self-learning local supervisions, the unanimous voting strategy is applied to eliminate some disapproving cluster divisions. Finally, the remaining more reliable cluster divisions are just a part of the data set. These self-learning local supervisions from visible layer are propagated to the inter-instance of hidden layer and reconstructed hidden layer. Then, some hidden features of the same local cluster tend to constrict together and some hidden features of different local clusters tend to disperse in the training process of sIsGRBM and sIsRBM.

B. Evaluation Setup

For three unsupervised clustering algorithms DP+sIsGRBM, K-means+sIsGRBM and AP+sIsGRBM algorithms based on the sIsGRBM model, we use three external evaluations that are accuracy[61], purity[62] and Fowlkes and Mallows Index (FMI)[63]. And we use accuracy[61], Rand index[64] and Fowlkes and Mallows Index (FMI)[63] to evaluate the other three unsupervised clustering algorithms DP+sIsRBM, K-means+sIsRBM and AP+sIsRBM algorithms based on the sIsRBM model.

In the training procedure of sIsGRBM and sIsRBM model, the parameter η is set to 0.4 and 0.5, respectively, and the learning rate is set to 10^{-4} and 10^{-5} , respectively.

1) *Accuracy*[61]: Given an instance x_i , let h_i and g_i be the cluster label and the true label, respectively. The clustering accuracy is given by:

$$AC = \frac{\sum_{i=1}^n \delta(g_i, \text{map}(h_i))}{n}, \quad (36)$$

where $AC \in [0, 1]$, n is the total number of instances, $\text{map}(r_i)$ maps each cluster label r_i to the equivalent label from the data set, and $\delta(x, y)$ equals to one if $x = y$ and equals to zero otherwise.

2) *Rand Index*[64]: The Rand index is one of the referential standards or absolute criteria of performance assessment for clustering data sets. Given a set $U = \{u_1, \dots, u_n\}$, n is the number of elements, $O = \{o_1, \dots, o_r\}$ is a partition of U with r subsets and $P = \{p_1, \dots, p_s\}$ is another partition of U with s subsets. Then the Rand index is defined as:

$$\text{Rand} = \frac{N_{ss} + N_{dd}}{N_{ss} + N_{sd} + N_{ds} + N_{dd}}, \quad (37)$$

where:

- N_{ss} is the number of pairs of elements in U that are in the same subset in O and in the same subset in P .
- N_{sd} is the number of pairs of elements in U that are in the same subset in O and in the different subsets in P .
- N_{ds} is the number of pairs of elements in U that are in the different subsets in O and to the same subset in P .
- N_{dd} is the number of pairs of elements in U that are in the different subsets in O and to the different subsets in P .

$\text{Rand} \in [0, 1]$. The value of Rand is close to 1 means that the partitions of O and P are more similar. In particular,

TABLE IV
THE ACCURACIES AND VARIANCE OF THE PROPOSED ALGORITHMS (DP+SLSGRBM, K-MEANS+SLSGRBM AND AP+SLSGRBM) AND CONTRASTIVE ALGORITHMS (DATASETS I).

Dataset (No.)	DP	K-means	AP	DP+GRBM	K-means+GRBM	AP+GRBM	DP+sLSGRBM	K-means+sLSGRBM	AP+sLSGRBM
BO (1)	0.4275±0.00000	0.4007±0.00068	0.4230±0.00000	0.4219±0.00014	0.3527±0.00012	0.4275±0.00001	0.4743±0.00340	0.4275±0.00009	0.4319±0.00033
WA (2)	0.4544±0.00000	0.4176±0.00007	0.3905±0.00000	0.4360±0.00046	0.4273±0.00001	0.4024±0.00017	0.4837±0.00290	0.4826±0.00180	0.4826±0.00240
WR (3)	0.4147±0.00000	0.4058±0.00005	0.4048±0.00000	0.5162±0.00009	0.4047±0.00120	0.4158±0.00000	0.5326±0.00076	0.5017±0.00210	0.4872±0.00002
BC (4)	0.4453±0.00000	0.4979±0.00000	0.4753±0.00000	0.4742±0.00055	0.4796±0.00055	0.4882±0.00075	0.5472±0.00140	0.5461±0.00083	0.5054±0.00330
VE (5)	0.5011±0.00000	0.4041±0.00110	0.4243±0.00000	0.4874±0.00015	0.4266±0.00009	0.4232±0.00000	0.5057±0.00230	0.5034±0.00880	0.4977±0.00440
AM (6)	0.5667±0.00000	0.3935±0.00650	0.3968±0.00000	0.5548±0.00110	0.4968±0.00790	0.3581±0.00003	0.5699±0.00008	0.5570±0.00045	0.5570±0.00033
VI (7)	0.5232±0.00000	0.4731±0.00001	0.4318±0.00000	0.4493±0.00025	0.4581±0.00023	0.4631±0.00038	0.5782±0.01220	0.5294±0.00510	0.5457±0.00340
WP (8)	0.5016±0.00000	0.4266±0.00029	0.4342±0.00000	0.4723±0.00019	0.4211±0.00001	0.4690±0.00011	0.5365±0.00720	0.5626±0.001210	0.5647±0.01460
VT (9)	0.4664±0.00000	0.3788±0.00130	0.4027±0.00000	0.4676±0.00017	0.3697±0.00170	0.4232±0.00021	0.5165±0.00000	0.6189±0.00000	0.6223±0.00002
Average	0.4779	0.4217	0.4207	0.4755	0.4263	0.4300	0.5276	0.5255	0.5216

TABLE V
THE PURITY OF THE PROPOSED ALGORITHMS (DP+SLSGRBM, K-MEANS+SLSGRBM AND AP+SLSGRBM) AND CONTRASTIVE ALGORITHMS (DATASETS I).

Dataset (No.)	DP	K-means	AP	DP+GRBM	K-means+GRBM	AP+GRBM	DP+sLSGRBM	K-means+sLSGRBM	AP+sLSGRBM
BO (1)	0.8778	0.8559	0.8731	0.8707	0.8785	0.8731	0.9014	0.8875	0.8945
WA (2)	0.8376	0.8175	0.8230	0.8427	0.8167	0.8282	0.8645	0.8660	0.8660
WR (3)	0.8089	0.8068	0.8028	0.8069	0.8056	0.8037	0.8297	0.8240	0.8298
BC (4)	0.8218	0.7325	0.7694	0.8344	0.7413	0.7667	0.8560	0.8086	0.8191
VE (5)	0.8339	0.8290	0.8327	0.8333	0.8317	0.8319	0.8591	0.8576	0.8589
AM (6)	0.7625	0.7571	0.7525	0.7626	0.7425	0.7635	0.7908	0.7815	0.7815
VI (7)	0.8490	0.8489	0.8493	0.8486	0.8482	0.8492	0.8780	0.8772	0.8778
WP (8)	0.7811	0.7709	0.7829	0.7811	0.7731	0.7687	0.8131	0.8181	0.8155
VT (9)	0.9179	0.9194	0.9201	0.9171	0.9196	0.9173	0.9495	0.9506	0.9510
Average	0.8323	0.8154	0.8229	0.8330	0.8175	0.8223	0.8603	0.8523	0.8549

TABLE VI
THE FOWLKES AND MALLOWS INDEX (FMI) OF THE PROPOSED ALGORITHMS (DP+SLSGRBM, K-MEANS+SLSGRBM AND AP+SLSGRBM) AND CONTRASTIVE ALGORITHMS (DATASETS I).

Dataset (No.)	DP	K-means	AP	DP+GRBM	K-means+GRBM	AP+GRBM	DP+sLSGRBM	K-means+sLSGRBM	AP+sLSGRBM
BO (1)	0.4471	0.3838	0.3999	0.4170	0.3767	0.4078	0.5110	0.4212	0.3992
WA (2)	0.4731	0.3907	0.4001	0.4660	0.3932	0.4011	0.4907	0.4781	0.4781
WR (3)	0.4093	0.4058	0.4104	0.4841	0.4053	0.4086	0.5281	0.4765	0.4676
BC (4)	0.4803	0.4632	0.4288	0.5140	0.4537	0.4342	0.5215	0.5199	0.4783
VE (5)	0.5044	0.4042	0.4149	0.4613	0.4052	0.4147	0.5117	0.4968	0.5046
AM (6)	0.5887	0.4341	0.4271	0.5719	0.4771	0.4074	0.5508	0.5151	0.5151
VI (7)	0.4963	0.4418	0.4357	0.5097	0.4422	0.4394	0.5600	0.5363	0.5552
WP (8)	0.5718	0.4148	0.4154	0.5027	0.4078	0.4362	0.5336	0.6782	0.6743
VT (9)	0.4644	0.4054	0.4212	0.4751	0.4041	0.4523	0.4964	0.6535	0.6557
Average	0.4928	0.4160	0.4170	0.4891	0.4184	0.4224	0.5227	0.5306	0.5253

TABLE VII
THE ACCURACIES AND VARIANCE OF THE PROPOSED ALGORITHMS (DP+SLSRBM, K-MEANS+SLSRBM AND AP+SLSRBM) AND CONTRASTIVE ALGORITHMS (DATASETS II).

Dataset (No.)	DP	K-means	AP	DP+RBM	K-means+RBM	AP+RBM	DP+sLSRBM	K-means+sLSRBM	AP+sLSRBM
HS (1)	0.5719±0.00000	0.5163±0.00013	0.5169±0.00001	0.5229±0.02400	0.5686±0.00140	0.5588±0.01620	0.6174±0.00480	0.6144±0.000410	0.5980±0.00390
QB (2)	0.5592±0.00000	0.5886±0.00000	0.5640±0.00000	0.6142±0.00003	0.5782±0.00087	0.5678±0.00095	0.6218±0.00000	0.6028±0.00016	0.6104±0.00003
SH (3)	0.6180±0.00000	0.5356±0.00000	0.5543±0.00000	0.5506±0.00018	0.5318±0.00018	0.5243±0.00011	0.7715±0.00200	0.5730±0.00018	0.5730±0.00250
SC (4)	0.6259±0.00000	0.5315±0.00011	0.5315±0.00000	0.8056±0.04390	0.5556±0.00014	0.5481±0.00200	0.8111±0.00210	0.5741±0.00001	0.5963±0.00004
BCW (5)	0.7909±0.00000	0.8541±0.00000	0.8541±0.00000	0.6362±0.00800	0.6309±0.00310	0.6309±0.00420	0.8524±0.02450	0.8682±0.00026	0.8664±0.00022
IR (6)	0.9067±0.00000	0.8933±0.00000	0.8867±0.00000	0.8333±0.00220	0.8333±0.00320	0.8200±0.00220	0.9800±0.09100	0.9667±0.02720	0.9467±0.02000
Average	0.6788	0.6532	0.6517	0.6605	0.6146	0.6083	0.7757	0.6999	0.6985

TABLE VIII
THE RAND INDEX OF THE PROPOSED ALGORITHMS (DP+SLSRBM, K-MEANS+SLSRBM AND AP+SLSRBM) AND CONTRASTIVE ALGORITHMS (DATASETS II).

Dataset (No.)	DP	K-means	AP	DP+RBM	K-means+RBM	AP+RBM	DP+sLSRBM	K-means+sLSRBM	AP+sLSRBM
HS (1)	0.5087	0.4989	0.4991	0.4994	0.5078	0.5053	0.5261	0.5246	0.5176
QB (2)	0.5066	0.5152	0.5077	0.5256	0.5118	0.5087	0.5292	0.5207	0.5239
SH (3)	0.5261	0.5007	0.5040	0.5033	0.5002	0.4993	0.6461	0.5088	0.5088
SC (4)	0.5308	0.5011	0.5011	0.6861	0.5053	0.5037	0.6930	0.5101	0.5177
BCW (5)	0.6686	0.7504	0.7504	0.5363	0.5335	0.5335	0.7479	0.7707	0.7681
IR (6)	0.8923	0.8797	0.8737	0.8322	0.8301	0.8213	0.9740	0.9575	0.9341
Average	0.6055	0.6077	0.6060	0.5972	0.5648	0.5620	0.6861	0.6321	0.6284

TABLE IX
THE FOWLKES AND MALLOWS INDEX (FMI) OF THE PROPOSED ALGORITHMS (DP+SLSRBM, K-MEANS+SLSRBM AND AP+SLSRBM) AND CONTRASTIVE ALGORITHMS (DATASETS II).

Dataset (No.)	DP	K-means	AP	DP+RBM	K-means+RBM	AP+RBM	DP+slsRBM	K-means+slsRBM	AP+slsRBM
HS (1)	0.5940	0.5519	0.5507	0.5534	0.5769	0.5726	0.6622	0.6598	0.6455
QB (2)	0.5586	0.5906	0.5625	0.5505	0.5511	0.5569	0.5743	0.5713	0.5751
SH (3)	0.6449	0.5933	0.6183	0.5842	0.5892	0.5824	0.7977	0.6117	0.6109
SC (4)	0.6784	0.6503	0.6504	0.8014	0.6536	0.6534	0.8315	0.6775	0.6844
BCW (5)	0.7455	0.7915	0.7915	0.7049	0.6976	0.6976	0.8080	0.8038	0.8012
IR (6)	0.8407	0.8208	0.8093	0.7637	0.7421	0.7398	0.9805	0.9554	0.9201
Average	0.6770	0.6664	0.6638	0.6597	0.6351	0.6338	0.7757	0.7132	0.7062

$Rand = 1$ means that the two data clusterings are exactly the same.

3) *Purity*[62]: The purity is used to measure the extent of each cluster contained data points from primarily one class. It is an external transparent evaluation measure for cluster quality. The purity is given by:

$$purity = \sum_{i=1}^K \frac{n_i}{n} P(S_i), P(S_i) = \frac{1}{n_i} \max_j (n_i^j), \quad (38)$$

where n_i^j is the number of the i -th input class that is assigned to the j -th cluster and S_i is a particular cluster size of n_i .

4) *Fowlkes and Mallows Index*[63]: The Fowlkes and Mallows index is an external evaluation method for two clusterings that can be defined as:

$$FMI = \sqrt{\frac{TP}{TP + FP} \times \frac{TP}{TP + FN}}, \quad (39)$$

where TP , FP and FN are the number of true positives, false positives and false negatives, respectively.

C. Unsupervised Clustering Performance on slsGRBM model

In this subsection, we use the self-learning local supervisions from image data sets to train the proposed slsGRBM with Gaussian linear visible layer units. The linear transformation is used to obtain reconstructed visible layer units from hidden layer units on the slsGRBM model. We compare the performance between three unsupervised clustering algorithms based on slsGRBM model that are termed as DP+slsGRBM, K-means+slsGRBM and AP+slsGRBM with three conventional algorithms DP, K-means and AP, respectively. Furthermore, we compare the performance between our slsGRBM model with traditional GRBM for clustering tasks.

1) *Comparison with Conventional Clustering Algorithms*: In Table IV, we present the unsupervised image clustering results on the MSRA-MM 2.0 data sets in Table II. The average accuracy of conventional clustering algorithms DP, K-means and AP are 0.4779, 0.4217 and 0.4207, respectively. But, the average accuracy of our proposed algorithms DP+slsGRBM, K-means+slsGRBM and AP+slsGRBM raise to 0.5276, 0.5255 and 0.5216, respectively. As a whole, DP+slsGRBM algorithm shows better clustering performance. Furthermore, there are seven data sets (BO, WA, WR, BC, VE, AM and VI) that obtain best clustering performance on the DP+slsGRBM algorithm. The other two data sets (WP and VT) obtain best clustering performance on the AP+slsGRBM

algorithm. The intuitive comparisons of the performance are shown in Fig. 2. In terms of the improvement extent of clustering performance, K-means+slsGRBM and AP+slsGRBM algorithms perform better. The average accuracy are raised as much as 24.61% and 23.98% by them. The intuitive comparisons of the average accuracy are shown in Fig. 5.

The results of purity are shown in Table V. The average purity of three traditional DP, K-means and AP are 0.8323, 0.8154 and 0.8229, respectively. But, they are raised to 0.8603, 0.8523 and 0.8549 by our DP+slsGRBM, K-means+slsGRBM and AP+slsGRBM algorithms, respectively. The DP+slsGRBM algorithm shows best performance. The intuitive comparisons of the performance are shown in Fig. 3 and Fig. 5.

The results of FMI are shown in Table VI. The average FMI of three traditional DP, K-means and AP are 0.4928, 0.4160 and 0.4170, respectively. But, they are raised to 0.5227, 0.5306 and 0.5253 by our DP+slsGRBM, K-means+slsGRBM and AP+slsGRBM algorithms, respectively. The K-means+slsGRBM algorithm shows best performance. For each individual data set, there are seven data sets (BO, WA, WR, BC, VE, AM and VI) show best performance on the DP+slsGRBM algorithm. The intuitive comparisons of the performance are shown in Fig. 4 and Fig. 5.

From above experimental results, our slsGRBM has powerful capability of feature learning and the hidden layer features of it show better clustering performance due to more reasonable feature distribution than original data.

2) *Comparison with Traditional GRBM*: Traditional GRBM also has the capability of feature extraction. We all want to know the self-learning local supervisions have more positive impact for hidden layer features of our slsGRBM model than traditional GRBM without any external interventions whether or not. So, it is necessary to compare traditional GRBM with our slsGRBM model using unsupervised clustering tasks. We also design another three unsupervised clustering algorithms that are termed as DP+GRBM, K-means+GRBM and AP+GRBM based on traditional GRBM which the hidden layer features of GRBM are the input of traditional unsupervised clustering algorithms DP, K-means and AP, respectively.

In Table IV, the average accuracies of DP+GRBM, K-means+GRBM and AP+GRBM algorithms based on traditional GRBM are 0.4755, 0.4263 and 0.4300, respectively. It is obviously that the clustering performances of them are worse than DP+slsGRBM, K-means+slsGRBM and AP+slsGRBM algorithms based on GRBM, respectively. As we can see from Table V and Table VI, whether the

purity or FMI, the algorithms based on our slsGRBM (DP+slsGRBM, K-means+slsGRBM and AP+slsGRBM) show better performances than the algorithms based on traditional GRBM (DP+GRBM, K-means+GRBM and AP+GRBM), respectively. The intuitive performance comparisons are shown in Figs. 2-5.

From above results, we have reason to believe that our slsGRBM has more rational hidden layer features distribution than traditional GRBM for unsupervised clustering tasks. So, the self-learning local supervisions bring more positive impact for feature extraction of our slsGRBM model with Gaussian linear visible layer units than traditional GRBM without any external interventions.

D. Unsupervised Clustering Performance on slsRBM model

In this subsection, we use the self-learning local supervisions from UCI data sets to train the proposed slsRBM with binary visible and hidden layer units. The sigmoid transformation is used to obtain reconstructed visible layer units from hidden layer units on the slsRBM model. We compare the performance between three unsupervised clustering algorithms based on slsRBM model that are termed as DP+slsRBM, K-means+slsRBM and AP+slsRBM with three conventional algorithms DP, K-means and AP, respectively. Further more, we compare the performance between our slsRBM model with traditional RBM for clustering tasks.

1) Comparison with Conventional Clustering Algorithms:

Table VII situates the results of the accuracy of three unsupervised clustering algorithms DP+slsRBM, K-means+slsRBM and AP+slsRBM based on the slsRBM model and three conventional clustering algorithms DP, K-means and AP on UCI data sets. For each data set in Table III, the DP+slsRBM algorithm shows best performance than all others in Table VII. The average accuracies of three conventional algorithms DP, K-means and AP are 0.6788, 0.6532 and 0.6517, respectively. However, the average accuracies of three algorithms DP+slsRBM, K-means+slsRBM and AP+slsRBM based on the slsRBM model are raised to 0.7757, 0.6999 and 0.6985, respectively. An intuitive comparison of accuracy for each data set is shown in Fig. 6. and for average accuracy of all data sets is shown in Fig. 9.

Table VIII situates the results of the rand index of all contrast algorithms. Obviously, the DP+slsRBM shows best clustering performance. The rand indices of three traditional algorithms DP, K-means and AP are 0.6055, 0.6077 and 0.6060, respectively. But, they are raised to 0.6861, 0.6321 and 0.6284 by the DP+slsRBM, K-means+slsRBM and AP+slsRBM algorithms, respectively. The intuitive comparisons of rand index are shown in Fig. 7 and Fig. 9. Table IX situates the results of the FMI of all contrast algorithms. The intuitive comparisons of FMI are shown in Fig. 8 and Fig. 9.

From above experimental results, our slsRBM for modeling the binary visible and hidden layer units also has powerful capability of feature learning and the hidden layer features of it show better clustering performance due to more reasonable feature distribution than original data.

2) *Comparison with Traditional RBM:* Traditional RBM also has powerful capability of feature learning. In the following, we compare the performance of traditional RBM and our slsRBM model using their hidden layer features as input of unsupervised clustering.

In Table VII, the average accuracies of three clustering algorithms DP+RBM, K-means+RBM and AP+RBM based on traditional RBM are 0.6605, 0.6146 and 0.6083, respectively. As a whole, they are obviously lower than DP+slsRBM, K-means+slsRBM and AP+slsRBM based on our slsRBM model. Tables VIII and IX situate the results of rand index and FMI evaluations. The algorithms based on our slsRBM model show better performance than the algorithms based on traditional RBM. The intuitive comparisons of them are shown in Figs. 6-9.

From above results, the self-learning local supervisions also bring more positive impact for feature extraction of our slsRBM model with binary visible and hidden layer units than traditional RBM without any external interventions.

VI. CONCLUSIONS

In this paper, we have proposed a powerful self-learning local supervision encoding framework for modeling binary or real-valued input data. No matter what type of input data, the hidden layer features stem from sigmoid transformation of the visible layer units and the reconstructed hidden features also stem from sigmoid transformation of the reconstructed visible layer units during sampling procedure. In the training procedure, the self-learning local supervisions have been used to constrict and disperse the distribution of the hidden layer features. We also have proposed two instantiations models based on this encoding framework: one is slsGRBM for modeling real-valued input data using linear transformation to obtain the reconstructed visible layer units from the hidden layer units and the other is slsRBM for modeling binary input data using sigmoid transformation to generate the reconstructed visible layer units from the hidden layer units.

The experimental results demonstrated the hidden layer features of our slsGRBM and slsRBM have more reasonable distribution than original input data for unsupervised clustering tasks. Furthermore, we proved the effectiveness of self-learning local supervisions for the proposed slsGRBM and slsRBM models by a comparison with traditional GRBM and RBM which have not any external interventions during the training process. The results showed that the self-learning local supervisions produce positive impact for optimizing the distribution of hidden layer features on our slsGRBM and slsRBM model and leads to a significant boost in unsupervised clustering performance.

VII. ACKNOWLEDGEMENT

This work were partially supported by the National Science Foundation of China (Nos. 61773324, 61573292) and the Fundamental Research Funds for the Central Universities (No. 2682015QM02)

REFERENCES

- [1] B. Yuan, J. Tu, R. W. Zhao, Y. Zheng, and Y. G. Jiang, "Learning part-based mid-level representation for visual recognition," *Neurocomputing*, 2017.
- [2] R. Socher, C. Y. Lin, A. Y. Ng, and C. D. Manning, "Parsing natural scenes and natural language with recursive neural networks," in *International Conference on International Conference on Machine Learning*, 2012, pp. 129–136.
- [3] J. Gao, J. Yang, G. Wang, and M. Li, "A novel feature extraction method for scene recognition based on centered convolutional restricted boltzmann machines," *Neurocomputing*, vol. 11, no. 2, pp. p14–19, 2016.
- [4] W. Diao, X. Sun, F. Dou, M. Yan, H. Wang, and K. Fu, "Object recognition in remote sensing images using sparse deep belief networks," *Remote Sensing Letters*, vol. 6, no. 10, pp. 745–754, 2015.
- [5] S. Choo and H. Lee, "Learning framework of multimodal gaussian-bernoulli rbm handling real-value input data," *Neurocomputing*, vol. 275, pp. 1813–1822, 2018.
- [6] K. Li, C. Zou, S. Bu, Y. Liang, J. Zhang, and M. Gong, "Multi-modal feature fusion for geographic image annotation," *Pattern Recognition*, vol. 73, 2017.
- [7] O. Ghahabi and J. Hernando, "Restricted boltzmann machines for vector representation of speech in speaker recognition," *Computer Speech and Language*, vol. 47, pp. 16–29, 2018.
- [8] C. L. P. Chen and S. Feng, "Generative and discriminative fuzzy restricted boltzmann machine learning for text and image classification," *IEEE Transactions on Cybernetics*, pp. 1–12, 2018.
- [9] A. Arinaldi and M. I. Fanany, "Kinematic features for human action recognition using restricted boltzmann machines," in *4th International Conference on Information and Communication Technology (ICoICT)*, 2016. IEEE, 2016, pp. 1–6.
- [10] G. Hinton and T. Sejnowski, "Learning and relearning in boltzmann machines," *Parallel distributed processing: Explorations in the microstructure of cognition*, vol. 1, pp. 282–317, 1986.
- [11] T. Tieleman, "Training restricted boltzmann machines using approximations to the likelihood gradient," in *International Conference on Machine Learning*, 2008, pp. 1064–1071.
- [12] G. E. Hinton, "Training products of experts by minimizing contrastive divergence," *Neural Computation*, vol. 14, no. 8, pp. 1771–1800, 2002.
- [13] D. Chen, J. Lv, and Z. Yi, "Graph regularized restricted boltzmann machine," *IEEE Transactions on Neural Networks and Learning Systems*, vol. PP, no. 99, pp. 1–9, 2017.
- [14] R. Sarikaya, G. E. Hinton, and A. Deoras, "Application of deep belief networks for natural language understanding," *IEEE/ACM Transactions on Audio, Speech, and Language Processing*, vol. 22, no. 4, pp. 778–784, 2014.
- [15] A. Krizhevsky, I. Sutskever, and G. E. Hinton, "Imagenet classification with deep convolutional neural networks," in *Advances in Neural Information Processing Systems*, 2012, pp. 1097–1105.
- [16] N. Lu, T. Li, X. Ren, and H. Miao, "A deep learning scheme for motor imagery classification based on restricted boltzmann machines," *IEEE Transactions on Neural Systems and Rehabilitation Engineering*, vol. PP, no. 99, pp. 1–1, 2016.
- [17] O. Fink, E. Zio, and U. Weidmann, "Fuzzy classification with restricted boltzmann machines and echo-state networks for predicting potential railway door system failures," *IEEE Transactions on Reliability*, vol. 64, no. 3, pp. 861–868, 2015.
- [18] Y. Chen, X. Zhao, and X. Jia, "Spectral-spatial classification of hyperspectral data based on deep belief network," *IEEE Journal of Selected Topics in Applied Earth Observations and Remote Sensing*, vol. 8, no. 6, pp. 2381–2392, 2015.
- [19] S. Elfving, E. Uchibe, and K. Doya, "Expected energy-based restricted boltzmann machine for classification," *Neural Networks*, vol. 64, pp. 29–38, 2015.
- [20] S. Nie, Z. Wang, and Q. Ji, "A generative restricted boltzmann machine based method for high-dimensional motion data modeling," *Computer Vision and Image Understanding*, vol. 136(C), pp. 14–22, 2015.
- [21] A. Graves, A.-r. Mohamed, and G. Hinton, "Speech recognition with deep recurrent neural networks," in *2013 IEEE International Conference on Acoustics, Speech and Signal Processing (ICASSP)*. IEEE, 2013, pp. 6645–6649.
- [22] J. Chu, H. Wang, H. Meng, P. Jin, and T. Li, "Restricted boltzmann machines with gaussian visible units guided by pairwise constraints," *IEEE Transactions on Cybernetics*, pp. 1–14, 2018.
- [23] Q. Yu, Y. Hou, X. Zhao, and G. Cheng, "Rényi divergence based generalization for learning of classification restricted boltzmann machines," in *2014 IEEE International Conference on Data Mining Workshop (ICDMW)*. IEEE, 2014, pp. 692–697.
- [24] C. Chen, C. Y. Zhang, L. Chen, and M. Gan, "Fuzzy restricted boltzmann machine for the enhancement of deep learning," *IEEE Transactions on Fuzzy Systems*, vol. 23, no. 6, pp. 2163–2173, 2015.
- [25] C. Ekanadham, S. Reader, and H. Lee, "Sparse deep belief net models for visual area v2," *Advances in Neural Information Processing Systems*, vol. 20, 2007.
- [26] A. Courville, G. Desjardins, J. Bergstra, and Y. Bengio, "The spike-and-slab rbm and extensions to discrete and sparse data distributions," *IEEE Transactions on Pattern Analysis and Machine Intelligence*, vol. 36, no. 9, pp. 1874–1887, 2014.
- [27] R. Karakida, M. Okada, and S.-i. Amari, "Dynamical analysis of contrastive divergence learning: Restricted boltzmann machines with gaussian visible units," *Neural Networks*, vol. 79, pp. 78–87, 2016.
- [28] M. R. Amer, T. Shields, B. Siddiquie, A. Tamrakar, A. Divakaran, and S. Chai, "Deep multimodal fusion: A hybrid approach," *International Journal of Computer Vision*, pp. 1–17, 2017.
- [29] Y. Lecun, Y. Bengio, and G. Hinton, "Deep learning," *Nature*, vol. 521, no. 7553, p. 436, 2015.
- [30] J. Zhang, G. Tian, Y. Mu, and W. Fan, "Supervised deep learning with auxiliary networks," in *the 20th ACM SIGKDD International Conference on Knowledge Discovery and Data Mining*. ACM, 2014, pp. 353–361.
- [31] H. Luo, P. Jia, S. Qiao, and S. Duan, "Enhancing electronic nose performance based on a novel qpso-rbm technique," *Sensors and Actuators B: Chemical*, vol. 259, pp. 241–249, 2018.
- [32] A. A. Alani, "Arabic handwritten digit recognition based on restricted boltzmann machine and convolutional neural networks," *Information*, vol. 8, no. 4, p. 142, 2017.
- [33] S. Bu, L. Wang, P. Han, Z. Liu, and K. Li, "3d shape recognition and retrieval based on multi-modality deep learning," *Neurocomputing*, vol. 259, pp. 183–193, 2017.
- [34] G. Cheng, P. Zhou, and J. Han, "Duplex metric learning for image set classification," *IEEE Transactions on Image Processing*, vol. 27, no. 1, pp. 281–292, 2017.
- [35] G. Chen, "Deep transductive semi-supervised maximum margin clustering," *arXiv preprint arXiv:1501.06237*, 2015.
- [36] K. T. Yesilbek and T. M. Sezgin, "Sketch recognition with few examples," *Computers and Graphics*, vol. 69, pp. 80–91, 2017.
- [37] R. Chen, S. Chen, M. He, D. He, and B. Tang, "Rolling bearing fault severity identification using deep sparse auto-encoder network with noise added sample expansion," *Proceedings of the Institution of Mechanical Engineers, Part O: Journal of Risk and Reliability*, vol. 231, no. 6, pp. 666–679, 2017.
- [38] S. Iso, S. Shiba, and S. Yokoo, "Scale-invariant feature extraction of neural network and renormalization group flow," *Phys. Rev. E*, vol. 97, p. 053304, May 2018.
- [39] C. T. Sari and C. Gunduz-Demir, "Unsupervised feature extraction via deep learning for histopathological classification of colon tissue images," *IEEE Transactions on Medical Imaging*, pp. 1–1, 2018.
- [40] M. A. Keyvanrad and M. M. Homayounpour, "Effective sparsity control in deep belief networks using normal regularization term," *Knowledge and Information Systems*, vol. 53, no. 2, pp. 533–550, 2017.
- [41] J. Yang, J. Deng, S. Li, and Y. Hao, "Improved traffic detection with support vector machine based on restricted boltzmann machine," *Soft Computing*, pp. 1–12, 2015.
- [42] X. Tang, N. Zhang, J. Zhou, and Q. Liu, "Hidden-layer visible deep stacking network optimized by pso for motor imagery eeg recognition," *Neurocomputing*, vol. 234, no. C, pp. 1–10, 2016.
- [43] H. B. Sailor, H. A. Patil, H. B. Sailor, and H. A. Patil, "Novel unsupervised auditory filterbank learning using convolutional rbm for speech recognition," *IEEE/ACM Transactions on Audio Speech and Language Processing*, vol. 24, no. 12, pp. 2341–2353, 2016.
- [44] P. Chopra and S. K. Yadav, "Restricted boltzmann machine and softmax regression for fault detection and classification," *Complex and Intelligent Systems*, vol. 4, no. 1, pp. 67–77, 2018.
- [45] X. Zhang, Y. Liang, C. Li, H. Ning, L. Jiao, and H. Zhou, "Recursive autoencoders-based unsupervised feature learning for hyperspectral image classification," *IEEE Geoscience and Remote Sensing Letters*, vol. 14, no. 11, pp. 1928–1932, 2017.
- [46] C. Xie, J. Lv, and X. Li, "Finding a good initial configuration of parameters for restricted boltzmann machine pre-training," *Soft Computing*, pp. 1–9, 2016.
- [47] H. Al-Dmour and A. Al-Ani, "A clustering fusion technique for mr brain tissue segmentation," *Neurocomputing*, vol. 275, pp. 546–559, 2018.
- [48] R. Stewart and S. Ermon, "Label-free supervision of neural networks with physics and domain knowledge," in *AAAI*, 2017, pp. 2576–2582.

- [49] S. M. Azimi, D. Britz, M. Engstler, M. Fritz, and F. Mcklich, "Advanced steel microstructural classification by deep learning methods," *Scientific Reports*, vol. 8, no. 1, 2017.
- [50] M. Seera, C. P. Lim, K. S. Tan, and S. L. Wei, "Classification of transcranial doppler signals using individual and ensemble recurrent neural networks," *Neurocomputing*, vol. 249, no. C, pp. 337–344, 2017.
- [51] K. Verma and R. K. Sharma, "Comparison of hmm- and svm-based stroke classifiers for gurmukhi script," *Neural Computing and Applications*, pp. 1–13, 2016.
- [52] K. A. Abdalmalak and A. Gallardo-Antolín, "Enhancement of a text-independent speaker verification system by using feature combination and parallel structure classifiers," *Neural Computing and Applications*, pp. 1–15, 2016.
- [53] H. Guan, T. Liu, J. Jiang, D. Tao, J. Zhang, H. Niu, W. Zhu, Y. Wang, J. Cheng, and N. A. Kochan, "Classifying mci subtypes in community-dwelling elderly using cross-sectional and longitudinal mri-based biomarkers," *Frontiers in Aging Neuroscience*, vol. 9, pp. 309–322, 2017.
- [54] M. Tahir, B. Jan, M. Hayat, S. U. Shah, and M. Amin, "Efficient computational model for classification of protein localization images using extended threshold adjacency statistics and support vector machines," *Computer Methods and Programs in Biomedicine*, vol. 157, 2018.
- [55] M. P. Hosseini, D. Pompili, K. Elisevich, and H. Soltanian-Zadeh, "Random ensemble learning for eeg classification," *Artificial Intelligence in Medicine*, 2018.
- [56] R. He, T. Tan, L. Davis, and Z. Sun, "Learning structured ordinal measures for video based face recognition," *Pattern Recognition*, vol. 75, pp. 4–14, mar 2018.
- [57] A. Rodriguez and A. Laio, "Clustering by fast search and find of density peaks," *Science*, vol. 344, no. 6191, pp. 1492–1496, 2014.
- [58] S. Lloyd, "Least squares quantization in pcm," *IEEE Transactions on Information Theory*, vol. 28, no. 2, pp. 129–137, 1982.
- [59] B. J. Frey and D. Dueck, "Clustering by passing messages between data points," *Science*, vol. 315, no. 5814, pp. 972–976, 2007.
- [60] H. Li, M. Wang, and X.-S. Hua, "Msra-mm 2.0: A large-scale web multimedia dataset," in *IEEE International Conference on Data Mining Workshops*. IEEE, 2009, pp. 164–169.
- [61] D. Cai, X. He, and J. Han, "Document clustering using locality preserving indexing," *IEEE Transactions on Knowledge and Data Engineering*, vol. 17, no. 12, pp. 1624–1637, 2005.
- [62] C. Ding, T. Li, W. Peng, and H. Park, "Orthogonal nonnegative matrix t-factorizations for clustering," in *the 12th ACM SIGKDD International Conference on Knowledge Discovery and Data Mining*. ACM, 2006, pp. 126–135.
- [63] R. Liu, H. Wang, and X. Yu, "Shared-nearest-neighbor-based clustering by fast search and find of density peaks," *Information Sciences*, vol. 450, pp. 200 – 226, 2018.
- [64] R. J. G. B. Campello, "A fuzzy extension of the rand index and other related indexes for clustering and classification assessment," *Pattern Recognition Letters*, vol. 28, no. 7, pp. 833–841, 2007.

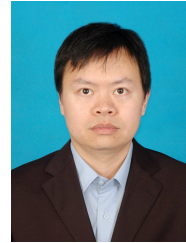


Jielei Chu received the B.S. degree from Southwest Jiaotong University, Chengdu, China in 2008, and is currently working toward the Ph.D. degree at Southwest Jiaotong University. His research interests are machine learning, data mining, semi-supervised learning and ensemble learning.



Tianrui Li (SM'11) received the B.S., M.S., and Ph.D. degrees in traffic information processing and control from Southwest Jiaotong University, Chengdu, China, in 1992, 1995, and 2002, respectively. He was a Post-Doctoral Researcher with Belgian Nuclear Research Centre, Mol, Belgium, from 2005 to 2006, and a Visiting Professor with Hasselt University, Hasselt, Belgium, in 2008; University of Technology, Sydney, Australia, in 2009; and University of Regina, Regina, Canada, in 2014.

He is currently a Professor and the Director of the Key Laboratory of Cloud Computing and Intelligent Techniques, Southwest Jiaotong University. He has authored or co-authored over 150 research papers in refereed journals and conferences. His research interests include big data, cloud computing, data mining, granular computing, and rough sets. Dr. Li is a fellow of the International Rough Set Society.



Hongjun Wang received his Ph.D. degree in computer science from Sichuan University of China in 2009. He is currently Associate Professor of the Key Lab of Cloud Computing and Intelligent Techniques in Southwest Jiaotong University. His research interests are machine learning, data mining and ensemble learning. He published over 30 research papers in journals and conferences and he is a member of ACM and CCF. He has a reviewer for several academic journals.



Jing Liu received his Ph.D. degree in management from Southwest Jiaotong University. She is currently an Assistant Professor of Business School in Sichuan University. Her research interests are machine learning, financial technology and modelling and forecasting high-frequency data.



Meng Hua received his Ph.D. degree in Mathematics from Sichuan University of China in 2010. His research interests include belief revision, reasoning with uncertainty, machine learning, general topology.